American Mineralogist, Volume 107, pages 509–516, 2022

Lazaraskeite, $Cu(C_2H_3O_3)_2$, the first organic mineral containing glycolate, from the Santa Catalina Mountains, Tucson, Arizona, U.S.A.

Hexiong Yang[1,*], Xiangping Gu[2], Ronald B. Gibbs[1], Stanley H. Evans[1], Robert T. Downs[1], and Zak Jibrin[1]

[1]Department of Geosciences, University of Arizona, 1040 East 4th Street, Tucson, Arizona 85721-0077, U.S.A.
[2]School of Geosciences and Info-Physics, Central South University, Changsha, Hunan 410083, China

Abstract

A new organic mineral species, lazaraskeite, ideally $Cu(C_2H_3O_3)_2$ with two polytypes M_1 and M_2, was discovered in the high elevation of the Santa Catalina Mountains, north of Tucson, Arizona, U.S.A. Both lazaraskeite-M_1 and -M_2 occur as euhedral individual crystals (up to 0.20 × 0.20 × 0.80 mm) or aggregates, with the former being more equant crystals and the latter bladed crystals elongated along the *c* axis. Associated minerals include chrysocolla, malachite, wulfenite, mimetite, hydroxylpyromorphite, hematite, microcline, muscovite, and quartz. Both polytypes are greenish-blue in transmitted light, transparent with white streak, and a vitreous luster. They are brittle and have a Mohs hardness of ~2; cleavage is perfect on {101}. No parting or twinning was observed. The measured and calculated densities are 2.12(2) and 2.138 g/cm^3, respectively, for lazaraskeite-M_1 and 2.10(2) and 2.086 g/cm^3 for lazaraskeite-M_2. Optically, lazaraskeite-M_1 is biaxial (−), with α = 1.595(3), β = 1.629(8), γ = 1.645(5), $2V_{meas}$ = 69(2)°, $2V_{cal}$ = 67°. Lazaraskeite-M_2 is also biaxial (−), with α = 1.520(5), β = 1.578(6), γ = 1.610(5), $2V_{meas}$ = 73(2)°, $2V_{cal}$ = 70°. Lazaraskeite is insoluble in water or acetone. An electron microprobe analysis for Cu and an Elemental Combustion System equipped with mass spectrometry for C yielded an empirical formula, based on 6 O apfu, $Cu_{1.01}(C_{1.99}H_{2.99}O_3)_2$ for lazaraskeite-M_1 and $Cu_{1.01}(C_{1.98}H_{3.00}O_3)_2$ for lazaraskeite-M_2. The measured $\delta^{13}C$ ‰ values are –37.7(1) and –37.8(1) for lazaraskeite-M_1 and -M_2, respectively.

Both lazaraskeite-M_1 and -M_2 are monoclinic with the same space group $P2_1/n$. The unit-cell parameters are *a* = 5.1049(2), *b* = 8.6742(4), *c* = 7.7566(3) Å, β = 106.834(2)°, *V* = 328.75(2) Å^3 for M_1 and *a* = 5.1977(3), *b* = 7.4338(4), *c* = 8.8091(4) Å, β = 101.418(2)°, *V* = 333.64(3) Å^3 for M_2. Lazaraskeite-M_1 is the natural analog of synthetic bis(glycolato)copper(II), $Cu(C_2H_3O_3)_2$. Its crystal structure is characterized by layers made of octahedrally coordinated Cu^{2+} cations and glycolate $(C_2H_3O_3)^-$ anionic groups. These layers, parallel to (101), are linked together by the strong hydrogen bonds (O-H···O = 2.58 Å). The CuO_6 octahedron is highly distorted, with four equatorial Cu-O bonds between 1.92 and 1.94 Å and two axial bonds at 2.54 Å. Lazaraskeite-M_2 has the same topology as lazaraskeite-M_1 and possesses all structural features of the low-temperature phase transformed from lazaraskeite-M_1 at 220 K (Yoneyama et al. 2013). The major differences between the two polytypes of lazaraskeite include: (1) M_1 has $b > c$, with β = 106.8°, whereas M_2 has $b < c$, with β = 101.4°; (2) the CuO_6 octahedron in M_1 is more elongated and distorted than in M_2; and (3) there is a relative change in the molecular orientation between the two structures.

Lazaraskeite represents the first organic mineral that contains glycolate. Not only does its discovery imply that more glycolate minerals may be found, but also suggests that glycolate minerals may serve as a potential storage for biologically fixed carbon.

Keywords: Lazaraskeite, organic mineral, glycolate, crystal structure, X-ray diffraction

Introduction

The commonly named "organic minerals" include simple and complex salts of different organic acids (such as formic, acetic, citric, mellitic, methanesulfonic, and oxalic acids), as well as numerous crystalline hydrocarbons, some amides, imides, porphyrines, triazolate complexes, and other compounds (e.g., Mills et al. 2009; Echigo and Kimata 2010). Among minerals derived from organic acids, oxalates are the most abundant class. In this study, we report a new organic mineral species, lazaraskeite, ideally $Cu(C_2H_3O_3)_2$, found in the high elevation of the mountains just north of Tucson, Arizona, U.S.A. Lazaraskeite possesses two polytypes, which are designated as lazaraskeite-M_1 and lazaraskeite-M_2 following the nomenclature guidelines recommended by the International Mineralogical Association (IMA) for "polytype" (or polymorph having the same topology). Lazaraskeite is the first organic mineral that contains glycolate. It is named after its finders, Warren G. Lazar and Beverly Raskin

* E-mail: hyang@arizona.edu

0003-004X/22/0003–509$05.00/DOI: https://doi.org/10.2138/am-2021-7895

Ross. Both Lazar and Raskin Ross enjoy prospecting, meteorite, and mineral hunting. The new mineral and its name have been approved by the Commission on New Minerals, Nomenclature and Classification (CNMNC) of IMA (IMA 2018-137). Part of the co-type samples have been deposited at the University of Arizona Mineral Museum (Catalog 22052 and 22381 for lazaraskeite-M_1 and -M_2, respectively) and the RRUFF Project (deposition R180026 and R190015).

Metal-glycolate solids have been an attractive subject of numerous studies. They are mostly prepared as intermediates of chemically and structurally controlled oxide particles (Day et al. 1996; Ksapabutr et al. 2004; Yu et al. 2007; Ng et al. 2008; Das et al. 2009; Pan et al. 2015; Takase et al. 2017, 2018) or metals (Chakroune et al. 2005; Anzlovar et al. 2008; Abdallah et al. 2015, 2018; Takahashi et al. 2016). They have also been investigated as intrinsic functional materials due to their lightness and various physicochemical properties. For example, their magnetocaloric properties at low temperatures make them valuable for cryogenic magneto-refrigeration applications (Chen et al. 2014) and their chelating properties for an enhanced reactivity in certain catalytic reactions, such as those involved in the polycondensation of ethylene glycol with bis-(hydroxyethyl)terephthalate for the production of poly(ethylene terephthalate)—an important thermoplastic material (Biros et al. 2002). Moreover, because of many coordination possibilities of glycolate molecules (such as bridging, chelating, and terminal modes) (Hubert-Pfalzgraf 1998), metal-glycolate compounds may exhibit different lattice dimensionalities (zero-, one-, two-, or three-dimensional) formed by metal polyhedra. Thus, structures based on isolated nanoclusters, chains, layers, or three-dimensional polymers, including three-dimensional lattices containing shape-controlled cages, can be obtained and their open structures can be used for gas storages or separations (Abdallah et al. 2018). This paper describes the physical and chemical properties of two polytypes of lazaraskeite and their crystal structures determined from the single-crystal X-ray diffraction data, demonstrating that lazaraskeite-M_1 is the natural analog of synthetic bis(glycolate)copper(II) $Cu(C_2H_3O_3)_2$ (e.g., Prout et al. 1968; Ye et al. 2010; Yoneyama et al. 2013, 2016) and lazaraskeite-M_2 the low-temperature phase of lazaraskeite-M_1 below 220 K (Yoneyama et al. 2013).

Sample description and experimental methods

Occurrence, physical, and chemical properties, and Raman spectra

Both lazaraskeite-M_1 and -M_2 were found on the western end of Pusch Ridge in the high elevation (975 m) of the Santa Catalina Mountains (32° 21′ 42″ N, 110° 57′ 30″ W), north of Tucson, Pima County, Arizona, U.S.A. They occur in a heavily fractured leucogranite, 3 to 5 feet below the surface (Fig. 1), with lazaraskeite-M_2 found in the relatively deeper area. Crystals of lazaraskeite-M_1 and -M_2 occur as individuals (up to 0.20 × 0.20 × 0.80 mm) or aggregates, but the former usually are found with a more equant morphology, and the latter as bladed crystals elongated along the *c* axis (Fig. 2). Associated minerals include chrysocolla, malachite, wulfenite, mimetite, hydroxylpyromorphite, hematite, microcline, muscovite, and quartz. Lazaraskeite is a secondary mineral believed to have formed through the interaction of fluids containing glycolic acid ($C_2H_4O_3$) with copper produced by the oxidation of primary and secondary minerals.

Both lazaraskeite-M_1 and -M_2 are greenish-blue in transmitted light, transparent with a white streak and vitreous luster, but crystals of lazaraskeite-M_2 appear to be relatively more pale-blue than those of lazaraskeite-M_1. They are brittle and have a Mohs hardness of ~2; cleavage is perfect on {101}. No parting or twinning was observed. The measured (by flotation in heavy liquids) and calculated densities for the two polytypes are given in Table 1. Optically, lazaraskeite-M_1 is biaxial (−), with $\alpha = 1.595(3)$, $\beta = 1.629(8)$, $\gamma = 1.645(5)$, $2V_{meas} = 69(2)°$, $2V_{cal} = 67°$, and the orientation $X \wedge c = 42°$, $Y = b$. The pleochroism is $X = Z$ = light blue-green and Y = blue-green, and the dispersion v > r (weak). Lazaraskeite-M_2 is also biaxial (−), with $\alpha = 1.520(5)$, $\beta = 1.578(6)$, $\gamma = 1.610(5)$, $2V_{meas} = 73(2)°$, $2V_{cal} = 70°$ and the orientation $X \wedge c = 36°$, $Y = b$. The pleochroism is $X = Z$ = pale blue and Y = greenish blue, and the dispersion v > r (weak). Lazaraskeite is insoluble in water or acetone. The compatibility indices for the two polytypes were not calculated because of the lack in a *k*-value for the glycolate group.

Figure 1. The pit where both lazaraskeite-M_1 and lazaraskeite-M_2 crystals were found. The tree right above the pit is a Foothill Palo Verde *Parkinsonia microphylla*. (Color online.)

The chemical compositions of lazaraskeite-M_1 and -M_2 were determined using a CAMECA SX-100 electron microprobe (WDS mode, 10 kV, 6 nA, and 5 μm beam diameter, 2 s counting) for Cu and an Elemental Combustion System equipped with mass spectrometry for C (Table 2), as well as $\delta^{13}C$‰. The resultant empirical chemical formula, calculated on the basis of 6 O apfu (from the structure determination), is $Cu_{1.01}(C_{1.99}H_{2.99}O_3)_2$ for lazaraskeite-M_1 and $Cu_{1.01}(C_{1.98}H_{3.00}O_3)_2$ for lazaraskeite-M_2, both of which can be simplified to $Cu(C_2H_3O_3)_2$. The measured $\delta^{13}C$‰ values are –37.7(1) and –37.8(1) for lazaraskeite-M_1 and -M_2, respectively. According to O'Leary (1988), such a value would result from C3-type plants with limiting carboxylation but fast diffusion. The predicted $\delta^{13}C$‰ value for such plants is –38. For the comparison, we also measured the $\delta^{13}C$‰ value from the roots that were intimately associated with lazaraskeite, which is –23.4(1), consistent with $\delta^{13}C_{VPDB}$‰ values of −20 to −37‰ for C3-type plants (Kohn 2010).

The Raman spectra of two lazaraskeite polytypes were collected from randomly oriented crystals on a Thermo-Almega microRaman system, using a solid-state laser with a wavelength of 532 nm and a thermoelectric cooled CCD detector. The laser is partially polarized with 4 cm^{-1} resolution and a spot size of 1 μm.

X-ray crystallography

The X-ray powder diffraction data of lazaraskeite were collected with a Rigaku D/Max 2500 diffractometer using Cu*K*α radiation (Online Materials[1]

Figure 2. A microscopic view of (**a**) lazaraskeite-M_2 and (**b**) lazaraskeite-M_1 crystals. (Color online.)

Table 1. Comparison of crystallographic data between lazaraskeite-M_1 and lazaraskeite-M_2

	lazaraskeite-M_1	Synthetic	lazaraskeite-M_2	Synthetic, at 150 K
Ideal chemical formula	$Cu(C_2H_3O_3)_2$	$Cu(C_2H_3O_3)_2$	$Cu(C_2H_3O_3)_2$	$Cu(C_2H_3O_3)_2$
Crystal symmetry	Monoclinic	Monoclinic	Monoclinic	Monoclinic
Space group	$P2_1/n$	$P2_1/n$	$P2_1/n$	$P2_1/n$
a (Å)	5.1049(2)	5.1095(9)	5.1977(3)	5.178(4)
b (Å)	8.6742(4)	8.677(2)	7.4338(4)	7.208(5)
c (Å)	7.7566(3)	7.746(1)	8.8091(4)	8.889(7)
β (°)	106.834(2)	106.841(2)	101.418(2)	100.840(9)
V (Å^3)	328.75(2)	328.7	333.64(3)	325.8(5)
a:b:c	0.59:1:0.89	0.60:1:0.89	0.70:1:1.19	0.72:1:1.23
Z	2	2	2	2
ρ_{meas} (g/cm^3)	2.12(2)		2.10(2)	
ρ_{cal} (g/cm^3)	2.138	2.138	2.086	2.177
2θ range for data collection	≤65.12	≤54.94	≤65.13	≤54.84
No. of reflections collected	4454	1978	4849	2356
No. of independent reflections	1192	747	1218	732
No. of reflections with $I>2\sigma(I)$	899	648	987	530
No. of parameters refined	64	62	64	64
R_{int}	0.026		0.024	0.068
Final R_1, wR_2 factors [$I>2\sigma(I)$]	0.027, 0.061	0.026, 0.070	0.024, 0.062	0.046, 0.117
Goodness-of-fit	1.010		1.064	1.118
Reference	(1)	(2)	(1)	(3)

Notes: References: (1) this study; (2) Ye et al. (2010); (3) Yoneyama et al. (2013).

Table 2. Determined chemical compositions (in wt%) for lazaraskeite-M_1 and lazaraskeite-M_2

Constituent	lazaraskeite-M_1 (Average of 6 analyses)	lazaraskeite-M_2 (Average of 7 analyses)	Standard
Cu	30.17(21)	29.98(22)	Chalcopyrite $CuFeS_2$
C	22.6(2)	22.2(2)	(1)
H	2.84	2.83	(2)
O	45.23	44.94	(2)
Total	100.84	99.95	

Notes: (1) The C contents of 22.6(2) and 22.2(2) wt% for lazaraskeite-M_1 and lazaraskeite-M_2, respectively, obtained from an Elemental Combustion System equipped with mass spectrometry, agree well with the ideal value of 22.49 wt%. The determined $\delta^{13}C$ ‰ value is −37.7(1) for lazaraskeite-M_1 and −37.8(1) for lazaraskeite-M_2. (2) The H and O contents were calculated based on the stoichiometry verified by the crystal structure determination. (3) The electron microprobe analysis data points for the two polytypes were obtained from several crystals because they were easily damaged by the electron beam, even with the moving stage and large electron beam size.

Table 3. Selected bond distances and angles in lazaraskeite

	Lazaraskeite M_1 (this study)	Lazaraskeite M_1 (Ye et al. 2010)	Lazaraskeite M_2 (this study)	Lazaraskeite M_2 at 150 K (Yoneyama et al. 2013)
	Distance (Å)	Distance (Å)	Distance (Å)	Distance (Å)
Cu-O1 × 2	1.9199(12)	1.920	1.9248(10)	1.934(4)
Cu-O2 × 2	1.9341(12)	1.936	1.9634(11)	1.959(4)
Cu-O3 × 2	2.5423(12)	2.546	2.4375(11)	2.432(4)
Average	2.1321	2.133	2.1085	2.109
C1-O1	1.265(2)	1.265	1.2623(18)	1.261(6)
C1-O3	1.248(2)	1.245	1.2506(17)	1.248(6)
C1-C2	1.510(2)	1.514	1.515(2)	1.516(9)
C2-H2	0.92(3)	0.91	0.98(3)	0.97(6)
C2-H3	0.94(2)	0.93	0.94(3)	0.83(5)
C2-O2	1.415(2)	1.421	1.4214(18)	1.431(7)
O2-H1	0.71(3)	0.76	0.93(2)	0.78(7)
<O1-C1-O3	123.34(14)°	123.38°	123.45(13)°	123.4(5)
<O1-C1-C2	118.07(14)°	118.10°	118.77(13)°	118.4(5)
<O3-C1-C3	118.57(14)°	118.51°	118.53(13)°	118.2(5)
<O2-C2-C1	108.53(14)°	108.48°	108.80(12)°	108.4(5)
O2···O3	2.5821(17)	2.579	2.5920(14)	2.604(6)
<O2-H1···O3	172(3)°	174.47°	172(2)°	167(4)

Table OM1). Unit-cell parameters refined from the powder data are a = 5.1041(4), b = 8.6705(8), c = 7.7508(6) Å, β = 106.747(5)°, and V = 328.46(3) Å^3 for lazaraskeite-$M1$, and a = 5.1916(2), b = 7.4048(4), c = 8.8036(5) Å, β = 101.462(4)°, and V = 331.69(1) Å^3 for lazaraskeite-M_2.

Single-crystal X-ray diffraction data for lazaraskeite were collected on a Bruker X8 APEX2 CCD X-ray diffractometer equipped with graphite-monochromatized Mo$K\alpha$ radiation from nearly equidimensional crystals (0.05 × 0.04 × 0.04 mm for lazaraskeite-M_1 and 0.06 × 0.06 × 0.05 mm for lazaraskeite-M_2) with frame widths of 0.5° in ω and 30 s counting time per frame. All reflections for both polytypes of lazaraskeite were indexed on the basis of a monoclinic unit cell (Table 1). The intensity data were corrected for X-ray absorption using the Bruker program SADABS. The systematic absences of reflections suggest the unique space group $P2_1/n$ for both polytypes. Their structures were solved and refined using SHELX2018 (Sheldrick 2015a, 2015b). All H atoms were located from the difference Fourier maps. The ideal chemistry was assumed during the refinements. The positions of all atoms were refined with anisotropic displacement parameters, except those for the H atoms, which were refined only with isotropic parameters. Final coordinates and displacement parameters of atoms in lazaraskeite are listed in CIF[1] (Online Materials) and selected bond-distances in Table 3.

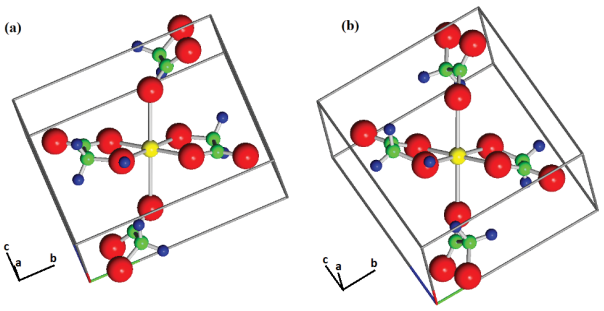

FIGURE 3. The Cu^{2+} octahedral coordination in (**a**) lazaraskeite-M_1 and (**b**) lazaraskeite-M_2. The red, yellow, green, and blue spheres represent O, Cu, C, and H atoms, respectively. (Color online.)

DISCUSSION

Crystal structures

Lazaraskeite-M_1 is the natural analog of synthetic bis(glycolato)copper(II), $Cu(C_2H_3O_3)_2$, which has been extensively studied for both its scientific and industrial interests (e.g., Prout et al. 1968; Ye et al. 2010; Yoneyama et al. 2013, 2016). Its crystal structure is characterized by layers of Cu^{2+} cations that are octahedrally coordinated to glycolate $(C_2H_3O_3)^-$ anionic groups (Figs. 3 and 4). These layers are parallel to (101), accounting for the perfect cleavage of the mineral, and are linked together by the relatively strong hydrogen bonding (O2-H1···O3 = 2.58 Å) (Fig. 5). Due to the Jahn-Teller effect, the CuO_6 octahedron is highly distorted, with four equatorial Cu-O bonds between 1.92 and 1.94 Å and two axial bonds at 2.54 Å.

Lazaraskeite-M_2 has the same topology as lazaraskeite-M_1 (Figs. 3, 4, and 5). However, the two polytypes also exhibit some noticeable structural differences. For example, lazaraskeite-M_1 has $b > c$, with $\beta = 106.8°$, whereas lazaraskeite-M_2 has $b < c$, with $\beta = 101.4°$ (Table 1). Moreover, the CuO_6 octahedron in lazaraskeite-M_1 is more elongated than that in lazaraskeite-M_2 (2.54 vs. 2.44 Å for the axial Cu-O bonds) (Table 3). There is also a relative change in the molecular orientation between the two structures, as shown in Figures 3 and 4.

By means of both single-crystal X-ray diffraction and magnetic measurements, Yoneyama et al. (2013) observed an isosymmetric structural transformation [or so-called "type 0" transition according to Christy (1995)] of synthetic lazaraskeite-M_1 at 220 K to a low-temperature phase. This phase transition, which is reversible and shows a large hysteresis (220–270 K), is marked by a discontinuous change in the paramagnetic susceptibility, unit-cell parameters (from $b > c$ to $c > b$), and axial Cu-O bonds in the elongated CuO_6 octahedra (from 2.54 to 2.44 Å). Isosymmetric structural phase transitions have been observed in several compounds, such as $(Mg_{0.75}Fe_{0.25})_2Si_2O_6$ orthopyroxene (Yang and Ghose 1995), $C_{13}H_{22}N^+ \cdot ClO_4^-$ (Wu and Jin 2013), and $LaGaO_3$ (Tang et al. 2018). Remarkably, the crystal structure of the low-temperature phase of lazaraskeite-M_1 at 150 K determined by Yoneyama et al. (2013) is identical to that of lazaraskeite-M_2 if the thermal effects due to the temperature difference are taken into account (Tables 1 and 3). Nonetheless, it is unclear why the two polytypes of lazaraskeite can occur in the same place. The chemical analyses on the two polytype crystals did not detect other elements except Cu and C. Perhaps, the different Eh or/and pH environments might play a role, as lazaraskeite-M_2 was found in a relatively deeper place (below 5 feet) than lazaraskeite-M_1. The obvious difference in crystal morphologies of the two polytypes appears to rule out the possibility that one structure form was transformed directly from the other. Interestingly, the coexistence of two polymorphs with the same symmetry and similar unit-cell parameters has been reported for the Cu-bearing organic compound $(\alpha\text{-pic})_2Cu(NO_3)_2$ (α-pic = 2-methylpyridine) (Cameron et al. 1972). Both forms of this material are monoclinic, space group $P2_1/c$, with unit-cell parameters $a = 8.31$, $b = 14.81$, $c = 14.14$ Å, $\beta = 123.9°$ (M_1) and $a = 8.57$, $b = 14.39$, $c = 14.20$ Å, $\beta = 119.5°$ (M_2).

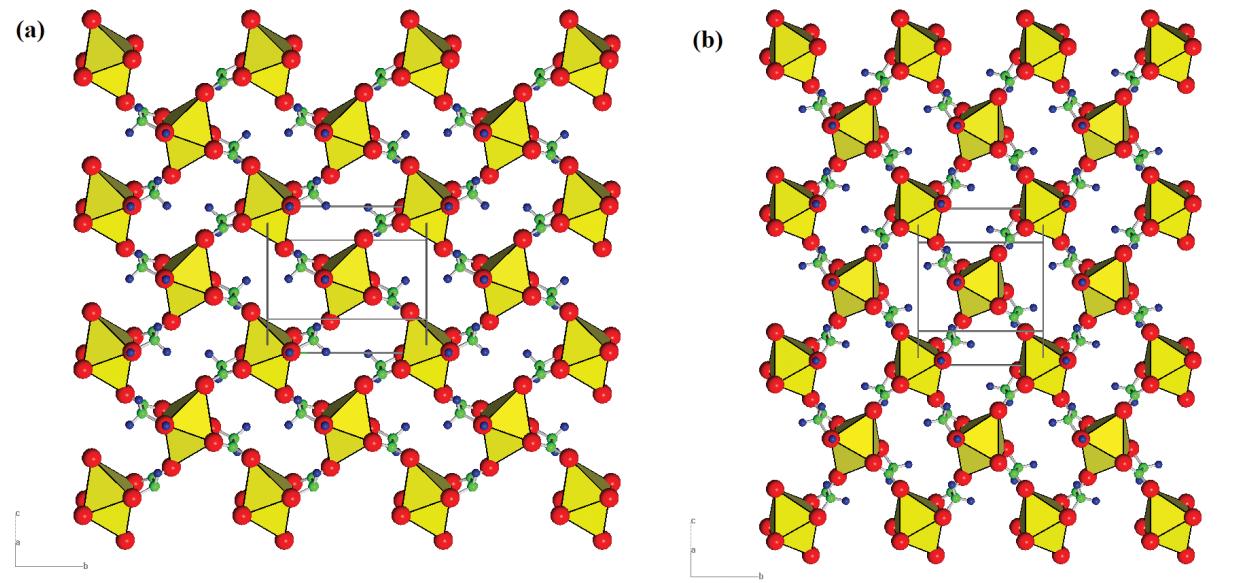

FIGURE 4. A layer, parallel to (101), formed by CuO_6 octahedra and glycolate $(C_2H_3O_3)^-$ ligands in (**a**) lazaraskeite-M_1 and (**b**) lazaraskeite-M_2. (Color online.)

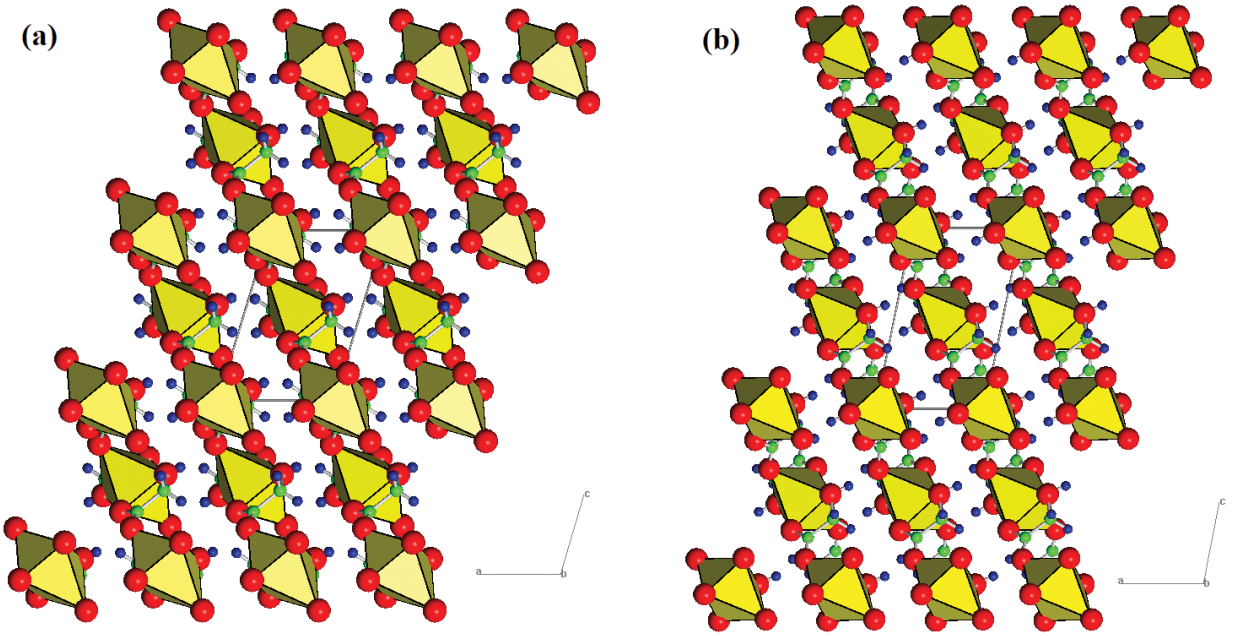

FIGURE 5. The structures of (**a**) lazaraskeite-M_1 and (**b**) lazaraskeite-M_2. The layers made of CuO_6 octahedra and glycolate $(C_2H_3O_3)^-$ ligands are linked together by hydrogen bonding along [101]. (Color online.)

Raman spectra

The Raman spectra of the two polytypes of lazaraskeite are shown in Figure 6. The strong resemblance between the two spectra is expected, as the structures of the two polytypes are similar. The difference in peak intensities between the two spectra principally results from the different crystal orientations when the data were collected. The tentative assignments of major Raman bands were made (Table 4) based on both experimental and theoretical spectroscopic studies on synthetic compounds containing the glycolic group $(C_2H_3O_3)^-$ (e.g., Medina et al. 2001; Silva et al. 2013; Gomes et al. 2014; do Nascimento et al. 2017). In particular, the bands between 1200–1670 cm^{-1} are attributed to the C-O and C-C stretching vibrations in the $C_2H_3O_3^-$ glycolic group and those from 840 to 1100 cm^{-1} to the C-OH stretching vibrations, as well as the O-C-O bending vibrations in $C_2H_3O_3^-$ glycolic group.

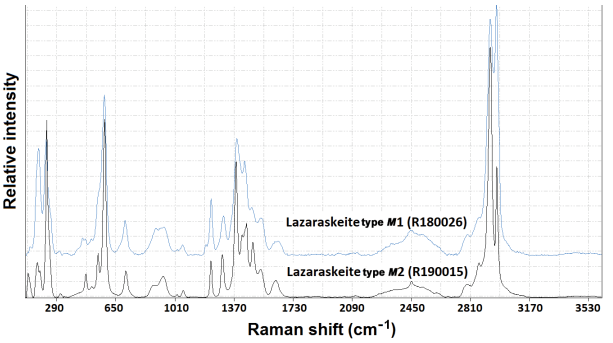

FIGURE 6. Raman spectra of lazaraskeite-M_1 and lazaraskeite-M_2.

TABLE 4. Tentative assignments of major Raman bands for lazaraskeite

Bands (cm^{-1})	Assignment
2760–3100	C-H and O-H stretching vibrations
2230–2650	O-H···O interaction
1200–1670	C-O and C-C stretching vibrations in the $C_2H_3O_3^-$ glycolic group
840–1100	C-OH stretching vibrations, as well as and O-C-O bending vibrations in $C_2H_3O_3^-$ glycolic group
400–800	Cu-O stretching vibrations, H-C-H bending vibrations, and C-C-O bending vibrations in $C_2H_3O_3^-$ glycolic group
<400	Lattice and O-Cu-O bending vibrational modes

Sources of glycolate

Many plants are known to produce glycolate during photorespiration in reactions catalyzed by glycolate oxidase or isocitrate lyase (Igamberdiev and Eprintsev 2016; Claassens et al. 2020 and references therein). However, whether such glycolate produced within plants can become available directly to form lazaraskeite in rocks several feet below the surface is unknown. Nevertheless, root exudates of many plants consist of a complex mixture of organic acid anions (including glycolic), phytosiderophores, sugars, vitamins, amino acids, purines, nucleosides, inorganic ions (e.g., HCO_3^-, OH^-, H^+), gaseous molecules (CO_2, H_2), and enzymes (e.g., Dakora and Phillips 2002; Engqvist et al. 2015). Plants take up most mineral nutrients through the rhizosphere where root exudates interact with microorganisms in soils and rocks. Thus, a possible formation mechanism for lazaraskeite occurs when plant root exudates containing glycolic acid encounter Cu-bearing minerals, such as chrysocolla, $(Cu_{2-x}Al_x)H_{2-x}Si_2O_5(OH)_4 \cdot nH_2O$, and malachite, $Cu_2(CO_3)(OH)_2$.

Numerous studies have demonstrated that glycolate can also be produced through the biodegradation of several organic materials by microorganisms under aerobic conditions (e.g., van Ginkel 1996; Liu et al. 2018; Fujiwara et al. 2020). In particular, Hunkeler and Aravera (2000) showed that glycolate is generated during the metabolic pathway of 1,2-dichloroethane

(DCA) degradation (from ethane → ethanol → glycolate → glyoxylate) by the aerobic bacterium *Xanthobacter autotrophicus* GJ10. Furthermore, they found that this degradation process is accompanied by a strong carbon isotope fractionation, with the produced inorganic carbon depleted significantly in ^{13}C ($\delta^{13}C$ = –46.2‰) and the biomass enriched in ^{13}C ($\delta^{13}C$ = –17.2‰), as compared to the initially added 1,2-DCA ($\delta^{13}C$ = –30.6‰). If we assume that aerobic microbial degradation of root exudates was involved in the formation of lazaraskeite, then the observation by Hunkeler and Aravera (2000) may render an explanation for the $\delta^{13}C$ value of –37.7‰ we measured for lazaraskeite.

Some microorganisms are also capable of producing glycolate (e.g., Burnap et al. 2015; Dellero et al. 2016; Taubert et al. 2019). For example, according to Eisenhut et al. (2008), the cyanobacterium *Synechocystis* has established three different routes for the metabolism of glycolate. One is similar to the bacterial glycolate metabolism, the second resembles the photorespiratory cycle found in higher plants, and the third involves the complete oxidation of glycolate to CO_2. As microorganisms are ubiquitous in nature, their contributions as a potential glycolate source for the formation of lazaraskeite should not be excluded.

Glycolate can be converted from oxalate, or vice versa, through the redox reactions either biotically or abiotically. In human bodies, the conversion between glycolate and oxalate is intimately associated with obesity and subsequent development of chronic diseases, as well as the formation of kidney stones (Knight et al. 2010). The conversion between glycolate and oxalate in metabolic pathways of plants is the key to the accumulations of biologically fixed carbon (Igamberdiev and Eprintsev 2016). Recently, the abiotic transition between glycolate and oxalate as a redox couple has attracted considerable attention because it demonstrates a carbon-neutral or CO_2-free energy circulation with the help of some metals or oxides as catalysts (Fukushima et al. 2018 and references therein). In Arizona, several oxalate minerals, such as weddellite ($CaC_2O_4 \cdot 2H_2O$), whewellite ($CaC_2O_4 \cdot H_2O$), and glushinskite ($MgC_2O_4 \cdot 2H_2O$), are abundant in decaying plants, especially cacti (e.g., Franceschi and Horner 1980; Horner and Wagner 1995; Prychid and Rudall 1999; Garvie 2003). These oxalate minerals are formed from elements released from the decaying plants by microorganisms. The $\delta^{13}C_{VPDB}$ values of the monohydrocalcite and calcite transformed from weddellite in the decaying Saguaro Cactus range from –1.65 to + 0.76‰, indicating that the carbon in weddellite was derived from atmospheric CO_2 (Garvie 2003). Accordingly, the possibility for oxalate in these minerals to be eventually converted abiotically to glycolate in lazaraskeite can be precluded, as the $\delta^{13}C_{VPDB}$ value we measured for lazaraskeite is –37.7‰.

Implications

A great number of glycolate compounds containing M^{n+} cations (n = 1, 2, 3, or 4) have been synthesized in laboratories, including lazaraskeite-M_1, $Ni(C_2H_3O_3)_2$, $Co(C_2H_3O_3)_2$, and $[Mg(C_2H_3O_3)(H_2O)_4]NO_3$ (e.g., Prout et al. 1968; Medina et al. 2000; Melikyan et al. 2000; Kang et al. 2004; Ye et al. 2010; Liu et al. 2011; Lin et al. 2013; Silva et al. 2013; Yoneyama et al. 2013; Gomes et al. 2014; Song and Hirato 2015; do Nascimento et al. 2017; Abdallah et al. 2018). In nature, glycolic acid ($C_2H_4O_3$) is a common and abundant organic matter that can be generated from several biological sources (see above). It is a product of fixed carbon accumulated in the conversion process of carbon compounds in metabolic pathways. The discovery of lazaraskeite, therefore, not only leads to the postulation that more glycolate minerals may be found but also implies that glycolate minerals may serve as a potential storage for biologically fixed carbon. Because glycolate is more stable in the reduced environments than oxalate, which usually forms various minerals on the ground surface or in decaying plants, we would expect more glycolate minerals, like lazaraskeite, to be found from the subsurface.

In addition to lazaraskeite-M_1 and lazaraskeite-M_2, the compound $Cu(C_2H_3O_3)_2$ appears to have another polymorph (designated as phase A for the simplicity of discussion) (Lin et al. 2013), which is dark blue in color and monoclinic with the same space group ($P2_1/n$) as lazaraskeite, but has a unit-cell volume twice that of lazaraskeite. The crystal structure of phase A exhibits many features similar to those in lazaraskeite, such as the coordination environments around Cu^{2+} cations and the layers formed by Cu^{2+} and $(C_2H_3O_3)^-$, which are linked together by hydrogen bonds. However, the CuO_6 octahedron in phase A is the most distorted and elongated of all three forms, with one axial Cu-O bond at 2.843 Å and the other at 2.642 Å. Compared to synthetic lazaraskeite-M_1, which can be obtained with solution reactions between 60–80 °C (Ye et al. 2010; Yoneyama et al. 2013), phase A was synthesized at a much higher temperature (120 °C) (Lin et al. 2013). Because lazaraskeite-M_1 transforms to lazaraskeite-M_2 at low temperature (Yoneyama et al. 2013), which is characterized by a significant shortening of the axial Cu-O bonds in the CuO_6 octahedron, it then begs the question of whether phase A can be attained by heating lazaraskeite-M_1, as the axial Cu-O bonds in phase are markedly longer than those in lazaraskeite-M_1.

Synthetic glycolate compounds $Ni(C_2H_3O_3)_2$ and $Co(C_2H_3O_3)_2$ have been regarded isostructural with lazaraskeite-M_1 (e.g., Medina et al. 2000; Kang et al. 2004; Nakane et al. 2018, 2020). However, a detailed structural comparison reveals that the NiO_6 and CoO_6 octahedra in $Ni(C_2H_3O_3)_2$ and $Co(C_2H_3O_3)_2$, respectively, are much less distorted than the CuO_6 octahedra in lazaraskeite-M_1, with all Ni-O bonds between 2.00 and 2.10 Å (Kang et al. 2004; Nakane et al. 2020) and Co-O bonds between 2.05 and 2.12 Å (Medina et al. 2000; Nakane et al. 2018). Moreover, the relative orientations between NiO_6/CoO_6 octahedra and glycolic groups in $Ni(C_2H_3O_3)_2$ and $Co(C_2H_3O_3)_2$ are more similar to those in lazaraskeite-M_2 rather than in lazaraskeite-M_1. Given these structural features, together with the fact that, like lazaraskeite-M_2, both $Ni(C_2H_3O_3)_2$ and $Co(C_2H_3O_3)_2$ have the unit-cell parameters $c > b$ (Medina et al. 2000; Kang et al. 2004; Nakane et al. 2018, 2020), not $b > c$ (like those for lazaraskeite-M_1), we suggest that these two Ni and Co compounds are better considered as analogs of lazaraskeite-M_2, instead of lazaraskeite-M_1. This consideration may also provide an explanation (at least in part) as to why no structural transformation was observed for $Ni(C_2H_3O_3)_2$ between 299 and 96 K (Nakane et al. 2020) or $Co(C_2H_3O_3)_2$ between 298 and 5 K (Nakane et al. 2018), in contrast to lazaraskeite-M_1, which undergoes a first-order phase transformation to lazaraskeite-M_2 at 220 K (Yoneyama et al. 2013).

Acknowledgments

This study was supported partially by Michael M. Scott.

References cited

Abdallah, A., Gaudisson, T., Sibille, R., Nowak, S., Cheikhrouhou-Koubaa, W., Shinoda, K., François, M., and Ammar, S. (2015) Structural and magnetic properties of mixed Co-Ln (Ln = Nd, Sm, Eu, Gd and Ho) diethyleneglycolate complexes. Dalton Transactions, 44, 16013–16023.

Abdallah, A., Ammar, S., Ban, V., Sibille, R., and Francois, M. (2018) Ab initio structure determination of $[Eu_5(C_2H_4O_2)_6(CH_3CO_2)_3]_n$ by X-ray powder diffraction. Acta Crystallographica, B74, 592–597.

Anzlovar, A., Orel, Z.C., and Zigon, M. (2008) Morphology and particle size of di(ethylene glycol) mediated metallic copper nanoparticles. Journal of Nanoscience and Nanotechnology, 8, 3516–3525.

Biros, S.M., Bridgewater, B.M., Villeges-Estrada, A., Tanski, J.M., and Parkin, G. (2002) Antimony ethylene glycolate and catecholate compounds: Structural characterization of polyesterification catalysts. Inorganic Chemistry, 41, 4051–4057.

Burnap, R.L., Hagemann, M., and Kaplan, A. (2015) Regulation of CO_2 concentrating mechanism in cyanobacteria. Life (Basel, Switzerland), 5, 348–371.

Cameron, A.F., Taylor, D.W., and Nuttall, R.H. (1972) Structural investigations of metal nitrate Complexes. Part III. Crystal and molecular structures of two crystalline forms of dinitratobis (α-picoline)copper(II). Dalton Transactions, 1, 58–63.

Chakroune, N., Viau, G., Ammar, S., Jouini, N., Gredin, P., Vaulay, M.J., and Fiévet, F. (2005) Synthesis, characterization and magnetic properties of disk-shaped particles of a cobalt alkoxide: $Co^{II}(C_2H_4O_2)$. New Journal of Chemistry, 29, 355–361.

Chen, Y.C., Guo, F.S., Liu, J.L., Leng, J.D., Vrabel, P., Orendac, M., Prokleska, J., Sechovsky, V., and Tong, M.L. (2014) Switching of the magnetocaloric effect of Mn-II glycolate by water molecules. Chemistry, 20, 3029–3035.

Christy, A.G. (1995) Isosymmetric structural phase transitions: Phenomenology and examples. Acta Crystallographica, B51, 753–757.

Claassens, N.J., Scarinci, G., Fischer, A., Flamholz, A.I., Newell, W., Frielingsdorf, S., Lenz, O., and Bar-Even, A. (2020) Phosphoglycolate salvage in a chemolithoautotroph using the Calvin cycle. Proceedings of the National Academy of Sciences, 117, 22452–22461.

Dakora, F.D., and Phillips, D.A. (2002) Root exudates as mediators of mineral acquisition in low nutrient environments. Plant and Soil, 245, 35–47.

Das, J., Evans, I.R., and Khushalani, D. (2009) Zinc glycolate: A precursor to ZnO. Inorganic Chemistry, 48, 3508–3510.

Day, V.W., Eberspacher, T.A., Frey, M.H., Klemperer, W.G., Liang, S., and Payne, D.A. (1996) Barium titanium glycolate: A new barium titanate powder precursor. Chemistry of Materials, 8, 330–332.

Dellero, Y., Jossier, M., Schmitz, J., Maurino, V.G., and Hodges, M. (2016) Photorespiratory glycolate–glyoxylate metabolism. Journal of Experimental Botany, 67, 3041–3052.

do Nascimento, A.L.C.S., Teixeira, J.A., Nunes, W.D.G., Gomes, D.J.C., Gaglieri, C., Treu-Filho, O., Pivatto, M., Caires, F.J., and Ionashiro, M. (2017) Thermal behavior of glycolic acid, sodium glycolate and its compounds with some bivalent transition metal ions in the solid state. Journal of Thermal Analysis and Calorimetry, 130, 1463–1472.

Echigo, T., and Kimata, M. (2010) Crystal chemistry and genesis of organic minerals: a review of oxalate and polycyclic aromatic hydrocarbon minerals. Canadian Mineralogist, 48, 1329–1358.

Eisenhut, M., Ruth, W., Haimovich, M., Bauwe, H., Kaplan, A., and Hagemann, M. (2008) The photorespiratory glycolate metabolism is essential for cyanobacteria and might have been conveyed endosymbiontically to plants. Proceedings of the National Academy of Sciences, 105, 17199–17204.

Engqvist, M.K.M., Schmitz, J., Gertzmann, A., Florian, A., Jaspert, N., Arif, M., Balazadeh, S., Mueller-Roeber, B., Fernie, A.R., and -Maurino, V.G. (2015) Glycolate oxidase3, a glycolate oxidase homolog of yeast L-lactate cytochrome c oxidoreductase, supports L-lactate oxidation in roots of Arabidopsis. Plant Physiology, 169, 1042–1061.

Franceschi, V.R., and Horner, H.T. Jr. (1980) Calcium oxalate crystals in plants. The Botanical Review, 46, 361–427.

Fujiwara, R., Noda, S., Tanaka, T., and Kondo, A. (2020) Metabolic engineering of *Escherichia coli* for shikimate pathway derivative production from glucose–xylose co-substrate. Nature Communications, 11, 279.

Fukushima, T., Kitano, S., Hata, S., and Yamauchi, M. (2018) Carbon-neutral energy cycles using alcohols. Science and Technology of Advanced Materials, 19, 142–152.

Garvie, L.A.J. (2003) Decay-induced biomineralization of the saguaro cactus (*Carnegiea gigantea*). American Mineralogist, 88, 1879–1888.

Gomes, D.J.C., Caires, F.J., Silva, R.C., Treu-Filho, O., and Ionashiro, M. (2014) Synthesis, characterization, thermal and spectroscopic studies of solidglycolate of light trivalent lanthanides, except promethium. Thermochimica Acta, 587, 33–41.

Horner, H.T., and Wagner, B.L. (1995) Calcium oxalate formation in higher plants. In S.R. Khan, Ed., Calcium Oxalate in Biological Systems, p. 53–72, CRC Press, Florida.

Hubert-Pfalzgraf, L.G. (1998) Some aspects of home and heterometallic alkoxides based on functional alcohols. Coordination Chemistry Reviews, 178-180, 967–997.

Hunkeler, D., and Aravera, R. (2000) Evidence of substantial carbon isotope fractionation among substrate, inorganic carbon, and biomass during aerobic mineralization of 1,2-dichloroethane by *Xanthobacter autotrophicus*. Applied and Environmental Microbiology, 66, 4870–4876.

Igamberdiev, A.U., and Eprintsev, A.T. (2016) Organic Acids: The Pools of Fixed Carbon Involved in Redox Regulation and Energy Balance in Higher Plants. Frontiers in Plant Science, 7, 1042–1015.

Kang, Q.-Q., Long, L.-S., Huang, R.-B., and Zheng, L.-S. (2004) Polymeric bis(glycolato)nickel(II). Acta Crystallographica, E60, 406–407.

Knight, J., Assimos, D.G., Easter, L., and Holmes, R.P. (2010) Metabolism of fructose to oxalate and glycolate. Hormone and -Metabolic Research = Hormon- Und Stoffwechselforschung = Hormones et Metabolisme, 42, 868–873.

Kohn, M.J. (2010) Carbon isotope compositions of terrestrial C3 plants as indicators of (paleo)ecology and (paleo)climate. Proceedings of the National Academy of Sciences, 107, 19691–19695.

Ksapabutr, B., Gulari, E., and Wongkasemjit, S. (2004) One-pot synthesis and characterization of novel sodium tris(glycozirconate) and cerium glycolate precursors and their pyrolysis. Materials Chemistry and Physics, 83, 34–42.

Lin, X.S., Sang, Y.L., Sun, W.D., and Yang, S.H. (2013) Assembly of three coordination polymers from glycolate ligands: syntheses, crystal structures, and thermal properties. Transition Metal Chemistry, 38, 503–509.

Liu, M., Ding, Y., Xian, M., and Zhao, G. (2018) Metabolic engineering of a xylose pathway for biotechnological production of glycolate in *Escherichia coli*. Microbial Cell Factories, 17, 51 1–11.

Liu, W., Wei, Z., and Yue, S. (2011) Tetraaqua(2-hydroxyacetato-κ^2 O^1,O^2)-magnesium nitrate. Acta Crystallographica, E67, m374.

Medina, G., Bernès, S., Martínez, A., and Gasque, L. (2001) Infrared assignment of bis(glycolato)-bis(pyridine) metal(ii) compounds and crystal structure of *trans*bis(glycolato)-*cis*-bis(pyridine)nickel(ii) dihydrate. Journal of Coordination Chemistry, 54, 267–284.

Medina, G., Gasque, L., and Bernés, S. (2000) Polymeric bis(glycolato)cobalt(II). Acta Crystallographica, C56, 637–638.

Melikyan, G.G., Amiryan, F., Visi, M., Hardcastle, K.I., Bales, B.L., Aslanyan, G., and Badanyan, S.H. (2000) Manganese(II):(III) glycolates: preparation, X-ray crystallographic study, and application in radical cycloaddition reactions. Inorganica Chimica Acta, 308, 45–50.

Mills, S.J., Hatert, F., Nickel, E.H., and Ferraris, G. (2009) The standardisation of mineral group hierarchies: application to recent nomenclature proposals. European Journal of Mineralogy, 21, 1073–1080.

Nakane, T., Yoneyama, S., Kodama, T., Kikuchi, K., Nakao, A., Ohhara, T., Higashinaka, R., Matsuda, T.D., Aoki, Y., and Fujita, W. (2018) Magnetic, thermal, and neutron diffraction studies of a coordination polymer: bis(glycolato)cobalt(II). Dalton Transactions, 48, 333–338.

Nakane, T., Aoyagi, S., and Fujita, W. (2020) Magnetic and thermal studies of a coordination polymer:bis(glycolato)nickel(II). New Journal of Chemistry, 44, 10519–10524.

Ng, S.H., Chew, S.Y., Santos, D.I., Chen, J., Wang, J.Z., Dou, S.X., and Liu, H.K. (2008) Hexagonal-shaped tin glycolate particles: A preliminary study of their suitability as Li-ion insertion electrodes. Chemistry—an Asian Journal, 3, 854–861.

O'Leary, M.H. (1988) Carbon isotopes in photosynthesis. BioScience, 38, 328–336.

Pan, G.H., Hayakawa, T., Nogami, M., Hao, Z., Zhang, X., Qu, X., and Zhang, J.H. (2015) Zinc titanium glycolate acetate hydrate and its transformation to zinc titanate microrods: synthesis, characterization and photocatalytic properties. RSC Advances, 5, 88590–88601.

Prout, C.K., Armstrong, R.A., Carruthers, J.R., Forrest, J.G., Murray-Rust, P., and Rossotti, F.J.C. (1968) Structure and stability of carboxylate complexes. Part I. The crystal and molecular structures of copper(II) glycolate, DL-lactate, 2-hydroxy-2-methylpropionate, methoxyacetate, and phenoxyacetate. Journal of the Chemical Society A: Inorganic, Physical, Theoretical, p. 2791–2813.

Prychid, C.J., and Rudall, P.J. (1999) Calcium oxalate crystals in Monocotyledons: A review of their structure and systematics. Annals of Botany, 84, 725–739.

Sheldrick, G.M. (2015a) SHELXT—Integrated space-group and crystal structure determination. Acta Crystallographica, A71, 3–8.

Sheldrick, G.M. (2015b) Crystal structure refinement with SHELX. Acta Crystallographica, C71, 3–8.

Silva, R.C., Caires, F.J., Gomes, D.J.C., Gigante, A.C., and Ionashiro, M. (2013) Synthesis, characterization and thermal studies of alkaline earth glycolate, except beryllium and radium. Thermochimica Acta, 573, 170–174.

Song, D., and Hirato, T. (2015) Fabrication of three-dimensional titania building blocks on glass substrate from mono-dispersed titanium glycolate spheres and their photocatalystic properties. Materials Transactions, 56, 348–352.

Takahashi, K., Yokoyama, S., Matsumoto, T., Huaman, J.L.C., Kaneko, H., Piquemal, J.-Y., Miyamura, H., and Balachandran, J. (2016) Towards a designed synthesis of metallic nanoparticles in polyols—elucidation of the redox scheme

in a cobalt-ethylene glycol system. New Journal of Chemistry, 40, 8632–8642.
Takase, K., Nishizawa, H., Imamura, K., Onda, A., Yanagisawa, K., and Yin, S. (2018) Synthesis of novel layered zinc glycolate and exchange of ethylene glycol with manganese acetate complex. Bulletin of the Chemical Society of Japan, 91, 1546–1552.
Takase, K., Nishizawa, H., Onda, A., Yanagisawa, K., and Yin, S. (2017) Synthesis and characterization of glycolate precursors to $MTiO_3$ ($M = Ni^{2+}$, Co^{2+}, Zn^{2}.). Journal of Asian Ceramic Societies, 5, 482–488.
Tang, Y.Q., López-Cartes, C., Avilés, M.A., and Córdoba, J.M. (2018) Isosymmetric structural phase transition of the orthorhombic lanthanum gallate structure as a function of temperature determined by Rietveld analysis. CrystEngComm, 20, 5562–5569.
Taubert, A., Jakob, T., and Wilhelm, C. (2019) Glycolate from microalgae: an efficient carbon source for biotechnological applications. Plant Biotechnology Journal, 17, 1538–1539.
van Ginkel, C.G. (1996) Complete degradation of xenobiotic surfactants by consortia of aerobic microorganisms. Biodegradation, 7, 151–164.
Wu, D.-H., and Jin, L. (2013) Temperature-induced isosymmetric reversible structural phase transition in triethylbenzylammonium perchlorate. Inorganic Chemistry Communications, 29, 151–156.
Yang, H., and Ghose, S. (1995) A transitional structural state and anomalous Fe-Mg order-disorder in Mg-rich orthopyroxene, $(Mg_{0.75}Fe_{0.25})_2Si_2O_6$. American Mineralogist, 80, 9–20.
Ye, Q.-S., Xie, M.-J., Liu, W.-P., Chen, X.-Z., Chang, Q.-W., and Yu, Y. (2010) Refinement of the crystal structure of bis(glycolato)copper(II), $Cu(C_2H_3O_3)_2$. Zeitschrift für Kristallographie, 225, 481–482.
Yoneyama, S., Kodama, T., Kikuchi, K., Kawabata, Y., Kikuchi, K., Ono, T., Hosokoshi, Y., and Fujita, W. (2013) Large structural transformation and ferromagnetic ordering in a coordination polymer with a two-dimensional square-planar lattice, bis(glycolato)copper(II). CrystEngComm, 15, 10193–10196.
Yoneyama, S., Kodama, T., Kikuchi, K., Fujisawa, T., Yamaguchi, A., Sumiyama, A., Shuku, Y., Aoyagi, S., and Fujita, W. (2016) Deuterium substitution effects on the structural and magnetic phase transitions of a hydrogen-bonded coordination polymer, bis(glycolato)copper(II). Dalton Transactions, 45, 16774–16778.
Yu, H.K., Eun, T.H., Yi, G.R., and Yang, S.M. (2007) Multi-faceted titanium glycolate and titania structures from room-temperature polyol process. Journal of Colloid and Interface Science, 316, 175–182.

Manuscript received November 16, 2020
Manuscript accepted February 28, 2021
Manuscript handled by G. Diego Gatta

Endnote:

[1]Deposit item AM-22-37895, Online Materials. Deposit items are free to all readers and found on the MSA website, via the specific issue's Table of Contents (go to http://www.minsocam.org/MSA/AmMin/TOC/2022/Mar2022_data/Mar2022_data.html). The CIF has been peer reviewed by our Technical Editors.